Journal of Materials Chemistry A

COMMUNICATION

View Article Online
View Journal | View Issue

Check for updates

Cite this: J. Mater. Chem. A, 2017, 5, 22125

Received 3rd August 2017
Accepted 3rd October 2017

DOI: 10.1039/c7ta06848d

rsc.li/materials-a

Published on 20 October 2017. Downloaded by Fudan University on 07/03/2018 07:17:25.

Tailorable coaxial carbon nanocables with high storage capabilities†

Guozhen Guan,‡ Jue Deng,‡ Jing Ren, Zhiyong Pan, Wen Zhuang, Sisi He, Bingjie Wang, Renchao Che and Huisheng Peng*

The preparation of nanomaterials into required sizes, structures and components is critical but remains challenging for practical applications. Here, coaxial nanocables were designed with the ability to be tailored into desired diameters, lengths and components through a low-cost, high-efficiency slicing process. The nanocables were radially grown from carbon nanotube cores with coaxial graphene or heteroatom-doped graphene sheet sheaths. This approach allowed the thickness to be fine-tuned, and the increased modulus from the sheath made the nanocables tailorable. The nanocables exhibited an aligned structure and were able to be cut into thin films with accurately controlled thicknesses ranging from tens of nanometers to micrometers while the two ends were left open. These nanocables are promising for the storage of materials and ions, and their incorporation into lithium-ion batteries demonstrates their high specific capacities.

Introduction

The manufacturing and processing of nanomaterials are critical for their properties and applications.[1–4] Ideally, nanomaterials should be fabricated to meet different requirements through mature technologies, and their aggregation structures should also be controllable to effectively extend their excellent properties to a macroscopic scale.[5,6] Although much effort has been devoted to advancing the preparation of nanomaterials in these directions, the low-cost and high-efficiency fabrication of nanomaterials remains challenging in application fields. For instance, one-dimensional nanotubes represent a major family of nanostructured materials that have been extensively studied for various promising applications. However, accurately controlling the manufacturing process to obtain precise sizes, components and aggregation structures, which is necessary to extend the properties of one-dimensional nanotubes from nanoscale to macroscopic-scale applications, is inherently difficult.[7–10]

In this communication, a new family of coaxial carbon nanocables (CNCs) is designed with the ability to be tailored into desired diameters, lengths and components through a low-cost, high-efficiency slicing process (Fig. 1). The CNCs are radially grown from carbon nanotube cores with coaxial graphene or heteroatom-doped graphene sheet sheaths. This approach allows the thickness to be fine-tuned, and the increased modulus from the sheath makes the CNCs tailorable. The CNCs exhibit an aligned structure and are able to be perpendicularly cut into thin films with accurately controlled thicknesses ranging from tens of nanometers to hundreds of micrometers while the two ends are left open. They are promising for the storage of materials and ions, and their incorporation into lithium-ion batteries demonstrates high specific capacities.

Experimental section

A silicon wafer sequentially coated with Al_2O_3 (10 nm) and iron (1 nm) layers was used to grow an aligned carbon nanotube array with a height of appropriately 2 mm in a quartz tube furnace (diameter of 1 inch, Thermo Scientific Lindberg/Blue M 1200 °C) at 750 °C by chemical vapor deposition.[11,12] The array was then transferred onto another clear silicon wafer inside the same tube furnace. The feeding gases included ethylene, hydrogen and argon with flowing speeds of 10, 10 and 130 cm^3 min^{-1}, respectively. The tube furnace was heated to 1060 °C within 23 min, and the graphene layers were coaxially grown on the outer surfaces of carbon nanotubes with increasing time from 15 to 120 min. The doping sources for the N-, S- and B-doped CNCs were acetonitrile, carbon disulfide and boron trichloride, respectively. The total sulfur and boron weight concentrations in the S-doped and B-doped CNCs were 0.7% and 0.3%, respectively. The resulting CNC arrays were embedded into a butyl alcohol/*N*,*N*-dimethylformamide

State Key Laboratory of Molecular Engineering of Polymers, Department of Macromolecular Science, Laboratory of Advanced Materials, Fudan University, Shanghai 200438, China. E-mail: penghs@fudan.edu.cn

† Electronic supplementary information (ESI) available. See DOI: 10.1039/c7ta06848d

‡ These authors contributed equally to this work.

Published on 20 October 2017. Downloaded by Fudan University on 07/03/2018 07:17:25.

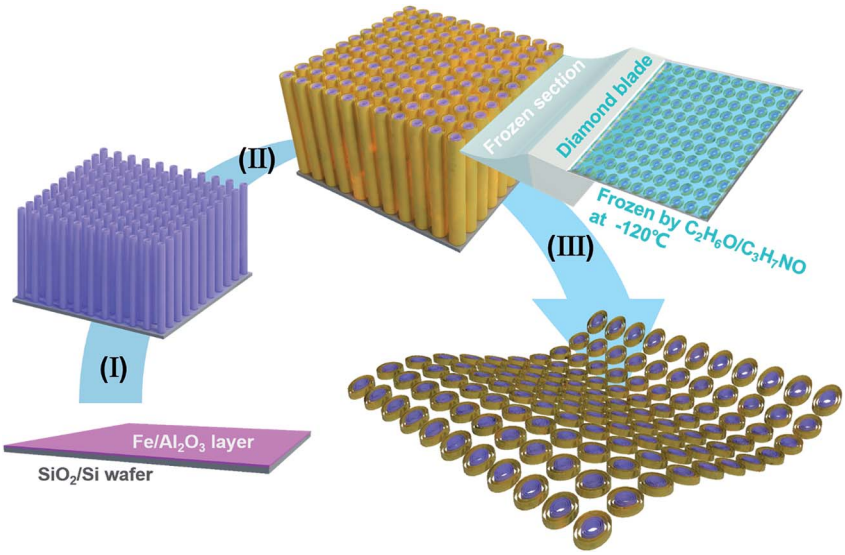

Fig. 1 Schematic of the synthesis and slicing process of a CNC array. (I) Aligned CNT arrays grown on the catalyst-modified silicon wafer. (II) Graphene layers with tunable thickness coaxially grown on the outer surfaces of CNTs. (III) Slicing the highly aligned CNC arrays by frozen sections.

mixture (volume ratio of 1/3) and frozen for sectioning by a diamond blade (Leica RM2265, Leica LN22).

Results and discussion

The resulting CNC arrays were able to be perpendicularly cut into thin and uniform slices. Almost no CNCs were pulled out of the array during the slicing process (Fig. 2a–c). In contrast, the pristine carbon nanotubes were unable to be perpendicularly cut because they were pulled out from the arrays under the same conditions. The CNCs displayed identical heights and had two open ends, and their thicknesses could be accurately controlled over a wide range from tens of nanometers to hundreds of micrometers (Fig. 2a–c).

The diameters of the CNCs could also be accurately controlled from 10 to 125 nm by increasing the growth time from 10 to 125 min during the second synthetic step (Fig. 2d–g and S1†). The newly grown graphene layers were concentrically wrapped around the pristine carbon nanotubes (Fig. S2†). We investigated the growth process and observed that the pyrolytic carbon atoms were deposited onto the templated carbon nanotubes and had formed uniform graphene layers (Fig. S3†). A variety of CNC patterns (Fig. 2h) were also prepared by fabricating catalyst layers with desired shapes to satisfy practical applications. For the CNCs, Raman spectroscopy showed that the I_{2D}/I_G decreased with increasing growth time (Fig. S4†), mainly due to the increasing thickness of graphene layers.[13–15] The close I_D/I_G value verified the similar degree of graphitization for different diameters. On the other hand, the larger diameters of CNCs resulted in the higher densities of CNC arrays, which was consistent with increasing typical peaks at 26° in the X-ray diffraction patterns (Fig. S5 and S6†). No peaks for impurity in the Raman spectra and X-ray diffraction patterns demonstrated the high purity of CNC arrays. The X-ray diffraction patterns from different directions revealed that the alignment in the original carbon nanotube array was maintained after the second growth step (Fig. S7†). Therefore, it can be confirmed that the re-grown graphene layers were loosely assembled on the outer sheath of the CNCs.

The CNC arrays with different diameters ranging from 20 to 120 nm can be cut tidily, and the resulting CNC slices showed integrated structures and open ends (Fig. 3a–c), which were critical for transportation and storage after the slicing process. When the CNCs were cut at different feeding speeds, the extents of plastic deformation were different. A lower feeding rate (*e.g.*, 0.2 mm s^{-1}) produced an irregular end after the slicing process (Fig. S8†), which would impede the transport and storage of both chemicals and ions. In contrast, tidy and open ends of CNC slices were maintained at a higher cutting speed of 20 mm s^{-1} (Fig. 3a–c). The mechanochemical slicing process of the CNCs was accompanied by the cleavage of the carbon–carbon bonds. The X-ray photoelectron spectra revealed that the graphite-like carbon atoms of the walls had been reduced from 69.4% to 66.2% after the CNCs were cut into slices. The percentage of carbon–oxygen groups, especially C–O, increased from 11.8% to 18.3% after cutting. Because this mechanochemical cleavage may have activated the carbon atoms near the fracture, the other molecules, such as oxygen, may have reacted with them to form oxygen-containing groups at the end (Fig. 3d and e).

The graphene layer can be further decorated with heteroatoms.[16–18] Here, the CNC was easily doped with N, B and S (Fig. 3f and S9†). Acetonitrile was used as a nitrogen and carbon source to grow the N-doped sheaths; the B- and S-doped sheaths were produced by using boron trichloride and carbon disulfide, respectively. Here, the N-doped CNCs were mainly studied as a model. The three peaks at 398.1, 401.2 and 403.3 eV in the X-ray photoelectron spectra indicated the three chemical states of the nitrogen atoms (Fig. 3f).[19,20] Accordingly, the percentages of graphitic nitrogen, pyridinic nitrogen and molecular

 This journal is © The Royal Society of Chemistry 2017

Published on 20 October 2017. Downloaded by Fudan University on 07/03/2018 07:17:25.

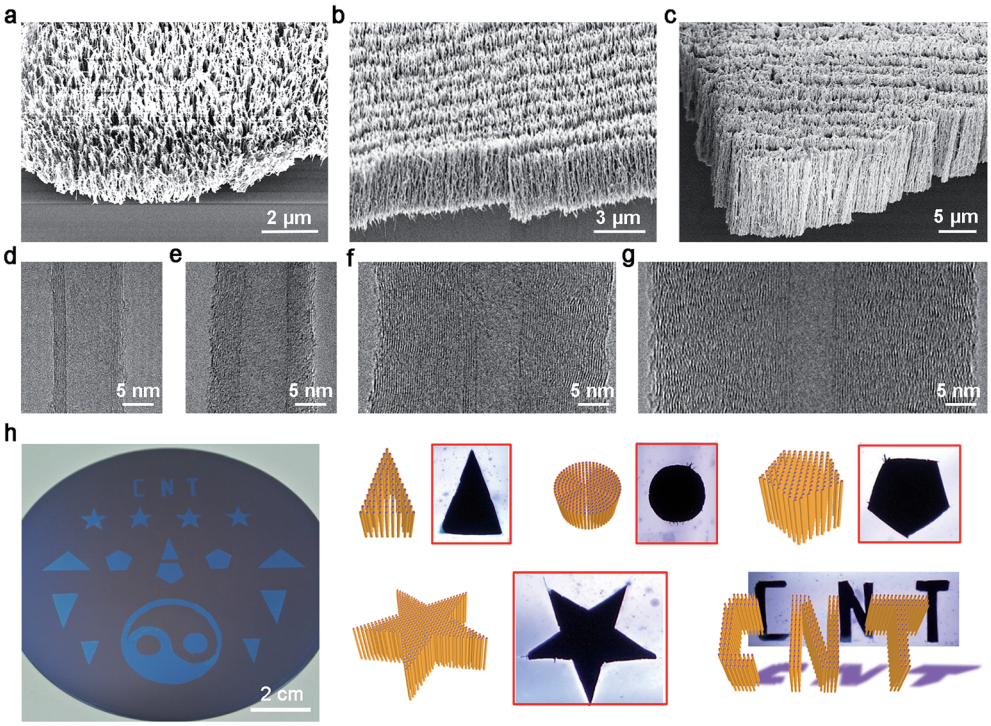

Fig. 2 Structural characterization of highly aligned CNC arrays. (a–c) SEM images of highly aligned CNC arrays with increasing heights of 1, 3 and 10 μm, respectively. (d–g) An original carbon nanotube and corresponding CNCs with increasing diameters of 8, 15, 35 and 50 nm with increasing growth times of 10, 30 and 45 min, respectively. (h) Photographs of patterned CNC arrays including a triangle, a circle, a regular pentagon, a pentagram and letters.

nitrogen were calculated to be 77.4%, 4.6% and 18.0%, respectively. The total nitrogen concentration in the N-doped CNCs was 6.2 wt%.

Because of their hollowness and the presence of inter lamellar space in their structure, carbon nanotubes have been proposed in a variety of applications; however, they have rarely

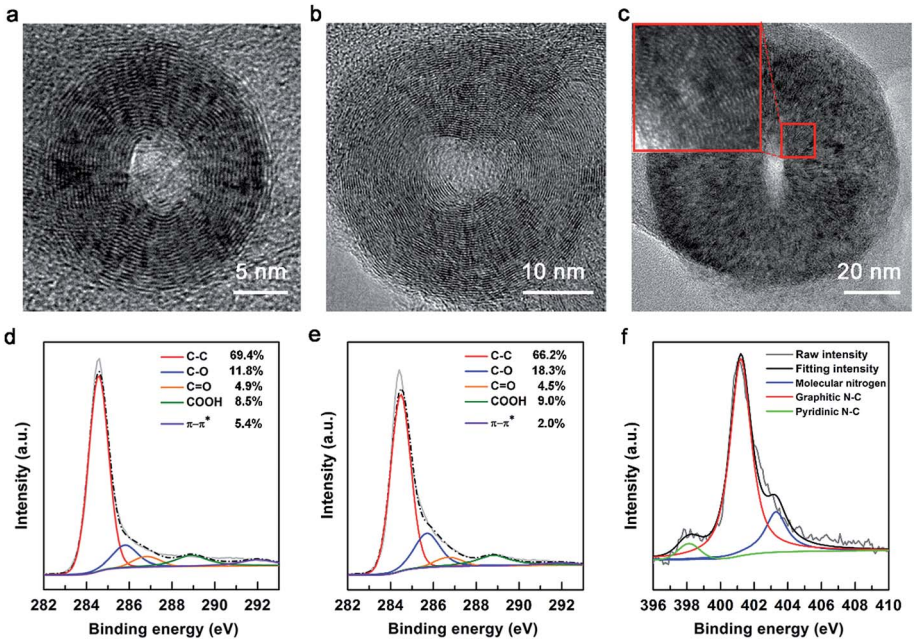

Fig. 3 CNCs with and without doping. (a–c) Cross-sectional images with increasing diameters of 20, 45 and 90 nm, respectively. (d and e) C 1s X-ray photoelectron spectroscopy of the highly aligned CNC arrays and CNC slices. The deconvoluted spectra at around 284.3 eV are resolved into different C peaks. (f) N 1s X-ray photoelectron spectrum of an aligned N-doped CNC array.

Published on 20 October 2017. Downloaded by Fudan University on 07/03/2018 07:17:25.

been used effectively in application fields. It is difficult for the transport of secondary phases inside the hollow structure and lamellar space of carbon nanotubes due to their closed ends and long pathways.[21–23] In the present study, open-ended CNCs could be efficiently filled with various substances, such as sublimed sulfur through gas-phase diffusion, phenyl-C_{61}-butyric acid methyl ester and polyvinylidene difluoride through liquid-phase capillarity of a solution or fused mass (Fig. S10†). The filling efficiencies (the total hollow space of the CNT divided by the occupied volume of the guest material) were calculated up to ~80% on the basis of the high-resolution transmission electron microscopy (TEM).

Smaller-sized ions can also be incorporated into the hollow parts of CNCs.[8,24,25] In the present work, we observed that the lamellar wall of the CNCs was critical for increasing the intercalation of ions. In addition, carbon materials have been widely used as electrode materials in lithium-ion batteries.[9,26–29] Here, the open ends and aligned structures of the CNC slices suggest that they are promising candidates for increasing the storage capacity and transport ability of lithium ions. The CNC slices were assembled with lithium metal into an electrochemical half-cell. In commercial batteries, graphite serves as an anode with a theoretical specific capacity of 372 mA h g^{-1} based on the intercalation model of C_6Li.[18,27,30] The specific capacities of the CNC slices increased with decreasing height because ion transport was more effective along shorter pathways and the hollow space was more fully utilized,[31–33] and they remained almost unchanged when the height was further decreased below 5 μm as no obvious differences existed for the above two factors (Fig. 4a). On the other hand, the reversible specific capacities almost stay the same with increasing diameter. The CNC slices with a height of 500 nm and a diameter of 60 nm reached a reversible specific capacity of ~1380 mA h g^{-1} at a rate of 0.2 A g^{-1}, which was ~7 times greater than that of the pristine carbon nanotube (200 mA h g^{-1}) at the same rate (Fig. 4a, b and S11†). The rate capabilities at 0.5, 1, 2 and 5 A g^{-1} were 1250, 1210, 1050 and 970 mA h g^{-1}, respectively (Fig. 4b and c). They show an improved performance and a better columbic efficiency compared with CNC arrays (Fig. S12†). The CNC slices also revealed a much better long-term cycling performance than CNC arrays before cutting; the specific capacity of the CNC slices even showed a slight increment after 500 cycles (Fig. 4d).

A comparison of the high-resolution TEM and lithium-ion-mapping energy-filtered TEM images verified that the lithium ions had extensively infiltrated both the hollow and lamellar spaces of the CNCs (Fig. 5a–c). In the charge/discharge curves, the potential plateaus were not distinguishable, implying the presence of multiple Li storage positions. The open-ended structures and low length/diameter ratios of CNCs favored the transport and storage of lithium ions in the inner space and among graphene layers. In addition, heteroatoms can further offer more defect or "host" sites for lithium intercalation.[29,34–36] The N-doped CNC slices (height of 500 nm, diameter of 60 nm) exhibited a specific capacity of 2450 mA h g^{-1} at a rate of 0.2 A g^{-1}, which is almost twice as large as that of the non-

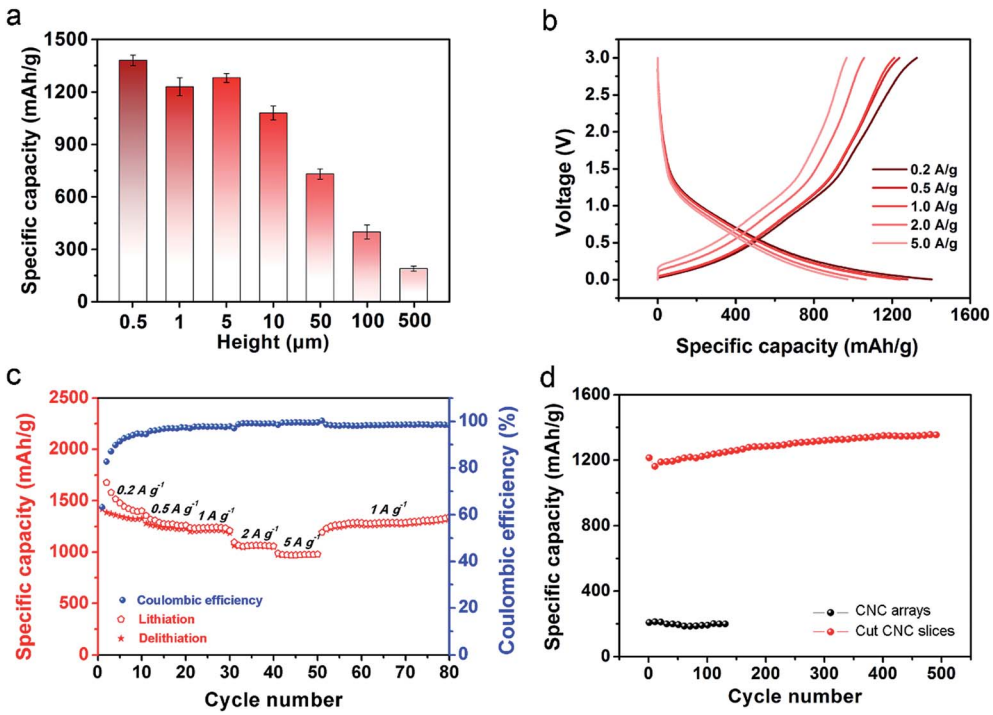

Fig. 4 Characterization of CNC slices for energy storage. (a) Specific capacities of the CNC slices (diameter of ~60 nm) with increasing heights at a current density of 1 A g^{-1}. (b) Charge and discharge curves of CNC slices at rates of 0.2, 0.5, 1, 2 and 5 A g^{-1}. (c) Reversible rate capability profiles of CNCs slices for the first 80 galvanostatic cycles with the coulombic efficiency being plotted on the right. The CNCs show a height of 500 nm and a diameter of 60 nm. (d) Cycle life of the CNC array and slice anodes at a rate of 1 A g^{-1}.

 This journal is © The Royal Society of Chemistry 2017

Published on 20 October 2017. Downloaded by Fudan University on 07/03/2018 07:17:25.

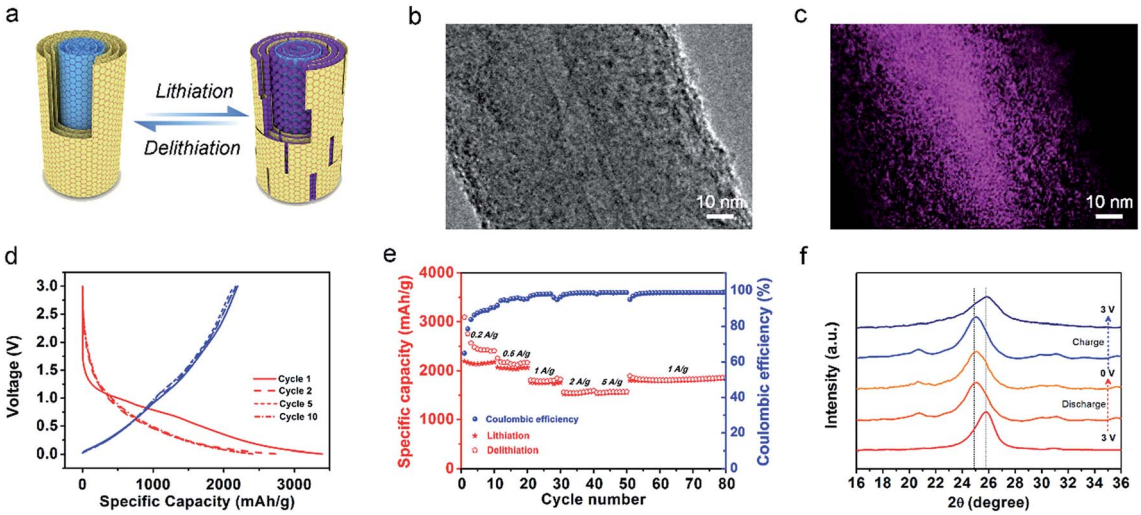

Fig. 5 Characterization and mechanism study of the N-doped CNCs in Li^+ storage. (a) Schematic illustration of a reversible lithiation and delithiation process of N-doped CNCs. (b) High-resolution TEM image of the N-doped CNC fully intercalated with lithium ions. (c) Electron energy loss spectroscopy mapping of lithium (rose red) in (b). (d) Charge and discharge curves of N-doped CNC slices at the 1st, 2nd, 5th and 10th cycles at a rate of 0.2 A g^{-1}. (e) Reversible rate capability profiles of N-doped CNC slices for the first 80 galvanostatic cycles. The coulombic efficiencies are plotted on the right. The N-doped CNCs show a height of 500 nm. (f) X-ray diffraction patterns of the CNCs in different charging and discharging states. The lithium ion is reversibly intercalated into the laminates of the CNC to increase the space between the laminates.

doped CNC slices at the same current rate (Fig. 5d). As expected, the charge–discharge curves remained almost unchanged during the cycling process. The specific capacities were 2140, 1790, 1600 and 1570 mA h g^{-1} at currents of 0.5, 1, 2 and 5 A g^{-1}, respectively, and the coulombic efficiencies exceeded 97% after the initial few circles at the current of 1 A g^{-1} (Fig. 5e and S12†).

In addition to the effective utilization of the hollow space, the lamellar distances of the newly grown graphene layers slightly expanded by 0.1 Å during the first cycle (Fig. S13†). This increase provided larger volumes for lithium-ion storage with higher delivery efficiencies during the introduction of lithium ions. During the delithiation process, the distance changes were irreversible during the first cycle but became reversible in the subsequent cycles[29,35] (Fig. 5f); the loosely assembled coaxial nanocable structure was critical for achieving high electrochemical performance in the resulting battery. Cyclic voltammetry was also used to investigate the electrochemical behavior of the CNCs during the circulation process (Fig. S14 and S15†). In the first scan, the peak at ~0.7 V is attributed to the formation of solid electrolyte interphase films, and N-doped CNC slices showed a higher peak intensity. The high intensity at ~0.7 V overlapped with the peak at 1.0–1.5 V, which made it hardly distinguishable. Actually, the peak current density at 1.0–1.5 V were similar for non-doped and N-doped CNC slices, but the peak currents of the N-doped CNC slices were much larger than those of the non-doped CNC slices.[29,35] A rather broad peak originated from sp^2-bonded carbons shifted from 0.25 to 0.15 V with increasing peak currents for a lower potential energy in delithiation, reflecting that the insertion and exclusion process expanded the nanoscale space between two neighboring graphene layers. The intensity of the sharp cathodic peak at 0.01 V, which is related to the lithiation process, remained unchanged. The two pairs of peaks also indicated high catalytic activity, which reflected the batteries' high coulombic efficiency.

Conclusions

In summary, a new family of CNC slices with tunable diameters, lengths and components is prepared by a general and efficient slicing process. The resulting CNC slices exhibit an aligned structure with the two ends left open after cutting. These novel CNC materials are promising for a variety of applications, and their use as electrodes of lithium-ion batteries is demonstrated with high specific capacities up to 2450 mA h g^{-1}.

Conflicts of interest

There are no conflicts to declare.

Acknowledgements

This work was supported by the Ministry of Science and Technology (2016YFA0203302), the National Natural Science Foundation of China (21634003, 51573027, 51403038, 51673043 and 21604012) and the Science and Technology Commission of Shanghai Municipality (16JC1400702, 15XD1500400 and 15JC1490200).

Notes and references

1 Y. Tang and M. Ouyang, *Nat. Mater.*, 2007, **6**, 754.
2 F. Yang, X. Wang, D. Zhang, J. Yang, D. Luo, Z. Xu, J. Wei, J. Wang, Z. Xu, F. Peng, X. Li, R. Li, Y. Li, M. Li, X. Bai, F. Ding and Y. Li, *Nature*, 2014, **510**, 522.

Published on 20 October 2017. Downloaded by Fudan University on 07/03/2018 07:17:25.

3 Q. Cao, S.-j. Han, G. S. Tulevski, Y. Zhu, D. D. Lu and W. Haensch, *Nat. Nanotechnol.*, 2013, **8**, 180.
4 L. Xu, W. Ma, L. Wang, C. Xu, H. Kuang and N. A. Kotov, *Chem. Soc. Rev.*, 2013, **42**, 3114.
5 M. Pumera, *Chem. Soc. Rev.*, 2010, **39**, 4146.
6 Y. Zhao, Y. Zhang, H. Sun, X. Dong, J. Cao, L. Wang, Y. Xu, J. Ren, Y. Hwang, I. H. Son, X. Huang, Y. Wang and H. Peng, *Angew. Chem., Int. Ed.*, 2016, **55**, 14384.
7 M. F. L. De Volder, S. H. Tawfick, R. H. Baughman and A. J. Hart, *Science*, 2013, **339**, 535.
8 H. Li, Y. Gong, C. Fu, H. Zhou, W. Yang, M. Guo, M. Li and Y. Kuang, *J. Mater. Chem. A*, 2017, **5**, 3875.
9 H. Wang, J. Wang, D. Cao, H. Gu, B. Li, X. Lu, X. Han, A. L. Rogach and C. Niu, *J. Mater. Chem. A*, 2017, **5**, 6817.
10 L. Yan, K. Wang, S. Luo, H. Wu, Y. Luo, Y. Yu, K. Jiang, Q. Li, S. Fan and J. Wang, *J. Mater. Chem. A*, 2017, **5**, 4047.
11 L. Qiu, J. Deng, X. Lu, Z. Yang and H. Peng, *Angew. Chem., Int. Ed.*, 2014, **53**, 10425.
12 H. Peng, X. Sun, F. Cai, X. Chen, Y. Zhu, G. Liao, D. Chen, Q. Li, Y. Lu, Y. Zhu and Q. Jia, *Nat. Nanotechnol.*, 2009, **4**, 738.
13 K. N. Kudin, B. Ozbas, H. C. Schniepp, R. K. Prud'homme, I. A. Aksay and R. Car, *Nano Lett.*, 2008, **8**, 36.
14 A. C. Ferrari, J. C. Meyer, V. Scardaci, C. Casiraghi, M. Lazzeri, F. Mauri, S. Piscanec, D. Jiang, K. S. Novoselov, S. Roth and A. K. Geim, *Phys. Rev. Lett.*, 2006, **97**, 187401.
15 Z. Sun, Z. Yan, J. Yao, E. Beitler, Y. Zhu and J. M. Tour, *Nature*, 2011, **471**, 124.
16 K. Gong, F. Du, Z. Xia, M. Durstock and L. Dai, *Science*, 2009, **323**, 760.
17 Z. S. Wu, A. Winter, L. Chen, Y. Sun, A. Turchanin, X. Feng and K. Muellen, *Adv. Mater.*, 2012, **24**, 5130.
18 Z. Pan, J. Ren, G. Guan, X. Fang, B. Wang, S.-G. Doo, I. H. Son, X. Huang and H. Peng, *Adv. Energy Mater.*, 2016, **6**, 1600271.
19 H. Wang, C. Zhang, Z. Liu, L. Wang, P. Han, H. Xu, K. Zhang, S. Dong, J. Yao and G. Cui, *J. Mater. Chem.*, 2011, **21**, 5430.
20 S. He, L. Qiu, L. Wang, J. Cao, S. Xie, Z. Zhang, J. Zhang, Y. Hu, B. Wang and H. Peng, *J. Mater. Chem. A*, 2016, **4**, 14968.
21 T. Takenobu, T. Takano, M. Shiraishi, Y. Murakami, M. Ata, H. Kataura, Y. Achiba and Y. Iwasa, *Nat. Mater.*, 2003, **2**, 683.
22 L. J. Li, A. N. Khlobystov, J. G. Wiltshire, G. A. D. Briggs and R. J. Nicholas, *Nat. Mater.*, 2005, **4**, 481.
23 Y. Nakanishi, H. Omachi, N. A. Fokina, P. R. Schreiner, R. Kitaura, J. E. P. Dahl, R. M. K. Carlson and H. Shinohara, *Angew. Chem., Int. Ed.*, 2015, **54**, 10802.
24 D. Deng, L. Yu, X. Chen, G. Wang, L. Jin, X. Pan, J. Deng, G. Sun and X. Bao, *Angew. Chem., Int. Ed.*, 2013, **52**, 371.
25 Y. Ma, R. Younesi, R. Pan, C. Liu, J. Zhu, B. Wei and K. Edström, *Adv. Funct. Mater.*, 2016, **26**, 6797.
26 B. Guo, X. Wang, P. Fulvio, M. Chi, S. Mahurin, X. Sun and S. Dai, *Adv. Mater.*, 2011, **23**, 4661.
27 R. Raccichini, A. Varzi, S. Passerini and B. Scrosati, *Nat. Mater.*, 2015, **14**, 271.
28 L. Dai, D. Chang, J. B. Baek and W. Lu, *Small*, 2012, **8**, 1130.
29 W. Shin, H. Jeong, B. Kim, J. Kang and J. Choi, *Nano Lett.*, 2012, **12**, 2283.
30 B. J. Landi, M. J. Ganter, C. D. Cress, R. A. DiLeo and R. P. Raffaelle, *Energy Environ. Sci.*, 2009, **2**, 638.
31 Q. Xiao, M. Gu, H. Yang, B. Li, C. Zhang, Y. Liu, F. Liu, F. Dai, L. Yang, Z. Liu, X. Xiao, G. Liu, P. Zhao, S. Zhang, C. Wang, Y. Lu and M. Cai, *Nat. Commun.*, 2015, **6**, 8844.
32 H. Han, T. Song, J.-Y. Bae, L. F. Nazar, H. Kim and U. Paik, *Energy Environ. Sci.*, 2011, **4**, 4532.
33 L. Zhou, D. Zhao and X. Lou, *Adv. Mater.*, 2012, **24**, 745.
34 L. Bulusheva, A. Okotrub, A. Kurenya, H. Zhang, H. Zhang, X. Chen and H. Song, *Carbon*, 2011, **49**, 4013.
35 W. Ren, D. Li, H. Liu, R. Mi, Y. Zhang and L. Dong, *Electrochim. Acta*, 2013, **105**, 75.
36 D. Li, L. Zhang, H. Chen, J. Wang, L.-X. Ding, S. Wang, P. J. Ashman and H. Wang, *J. Mater. Chem. A*, 2016, **4**, 8630.

 This journal is © The Royal Society of Chemistry 2017